

Atom-Generated Spatial Multi-Mode Structure of Squeezed Light

Mi Zhang,¹ R. Nicholas Lanning,² Zhihao Xiao,² Jonathan P. Dowling,² Irina Novikova,¹ and Eugeniy E. Mikhailov^{1,*}

¹Department of Physics, College of William & Mary, Williamsburg, Virginia 23187, USA

²Department of Physics & Astronomy, Louisiana State University, Baton Rouge, Louisiana 70803, USA

(Dated: April 23, 2022)

We generate a squeezed vacuum field via an interaction between a laser beam and an atomic ensemble. A measurement of the quantum noise of a spatially modified squeezed field is conducted. We find the noise suppression to be greatly affected by the transverse profile of the spatial mask and its position along the propagation direction. We have developed a multimode model to describe the mode structure of the light fields which qualitatively explains the quadrature noise behavior in terms of higher-order Laguerre-Gauss modes.

PACS numbers: 42.50.Lc, 42.50.Nn

Understanding of the spatial mode composition of optical fields is crucial for many quantum applications [1]. For example, multimode squeezing and entanglement is necessary for quantum imaging [2, 3], quantum information multiplexing [4, 5], hyperspectral encoding, etc. At the same time, the presence of several spatial modes may be detrimental for quantum-enhanced measurements [6]. For example, if the quadrature angle, corresponding to the maximum quantum noise suppression, is different for different spatial modes, the overall minimum noise may be increased, even if each individual spatial mode is squeezed. If the proper mode structure is identified, however, it may be possible to extract a single squeezed mode and eliminate others by means of an efficient spatial mode sorter [7] or to tailor the apparatus [8] to further boost the signal-to-noise ratio (SNR). In this way we would be able to produce single, maximally squeezed, higher-order modes upon demand.

In this Letter we investigate the spatial properties of the resonant optical field after interaction with dense Rb vapor under the conditions for polarization self-rotation (PSR) [9–11]. It is known that in the case of a linearly polarized input field, the noise in the orthogonal polarization is modified, leading to the generation of squeezed vacuum [12–14]. Several experiments demonstrated up to 3 dB of quantum noise suppression with this scheme [15–17]. There is still an open question, however, why better quantum noise suppression cannot be experimentally achieved, in contrast to the predictions of the theory [12, 18, 19]. Here we present a study of the spatial mode structure of the output optical fields in the PSR squeezing process, that gives strong evidence of its multimode nature. In particular, we carried out a simple sorting of the spatial modes, elucidating the mode structure of the pump and the squeezed field, and developed an intuitive theoretical description of the higher-order generation, that qualitatively agrees with the experiment.

The experimental setup for squeezing generation, depicted at the Fig. 1, is similar to one used in our previous experiments [20]. An extended cavity diode laser was red detuned by approximately 100 MHz from the

$5^2S_{1/2}, F = 2 \rightarrow 5^2P_{1/2}, F' = 2$ transition of the ^{87}Rb ($\lambda \simeq 795$ nm). The laser output was spatially filtered by passing it through a single-mode-polarization-maintaining (SMPM) fiber and linearly polarized using a Glan-laser polarizer (GP) and focused into a 7.5 cm long cylindrical Pyrex cell with isotropically enriched ^{87}Rb vapor and no buffer gas. The waist of the focused beam (diameter $100 \mu\text{m}$ at $1/e^2$ intensity level) was located 6.5 cm away from the front of the cell. The cell was mounted inside three layer μ -metal magnetic shielding, and maintained at a constant temperature of 66°C , corresponding to the Rb density at $5.4 \times 10^{11} \text{ cm}^{-3}$.

The interaction of a strong laser field with atoms modifies the vacuum fluctuations in the orthogonal polarization. To measure their quadrature noise we mixed the two fields at the polarization beam splitter (PBS) after their polarizations were rotated by 45° and sent them to

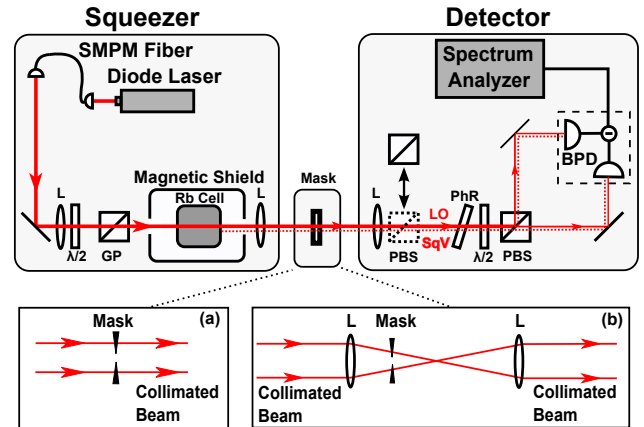


FIG. 1. (Color online) Experimental setup. SMPM fiber depicts single-mode polarization-maintaining fiber, $\lambda/2$ is half-wave plate, GP is Glan-laser polarizer, PBS is a polarizing beam splitter, PhR is a phase-retarding wave plate, and BPD is a balanced photodetector. In the experiment a mask was inserted either in the collimated beam (a) or in the focused beam (b).

a balanced photodiode (BPD), realizing a homodyne detection in which the strong laser field served as the local oscillator (LO) [15, 17]. Their relative phase (quadrature angle) was adjusted by tilting the phase-retarding (PhR) plate (a birefringent quarter-wave plate with a crystal axis set parallel to the LO polarization). All the quantum measurements reported below were performed at 1 MHz detection frequency with 100 kHz resolution and 30 Hz video bandwidths. To calibrate the SQL (Standard Quantum Limit, i.e., shot-noise) level, we inserted an additional PBS into the beam after the cell, which reflects the squeezed field and passes only the LO field. We detected noise suppression of 1.9 ± 0.2 dB below the SQL level in the maximally squeezed quadrature and 11 dB of anti-squeezing in the orthogonal quadrature (see Fig. 2 at 100% transmission level), which is quite typical for these kinds of atomic squeezers.

All previous experimental and theoretical analysis of SPR squeezing assumed an identical single spatial for both the strong pump and vacuum fields, with either fundamental Gaussian [15, 17] or Laguerre-Gaussian [20] transverse profiles. However, as we show below, the spatial composition of the squeezed field mode is more complex.

In order to investigate the spatial property of the squeezed field, we inserted different radially symmetric spatial masks into the beam after the Rb cell, as shown in Fig. 1(a). We classify the beam masks as irises or disks, depending if they block the outer or inner part of the laser beam. We used an adjustable iris, and a set of fixed sizes disks. These masks were inserted into the collimated part of the laser beam after interaction with the atoms, making sure that the masks are properly centered. Since the masks reduced the LO power, we carefully recalibrated the shot-noise level for every mask and adjusted the phase retarding plate to track the maximally squeezed and anti-squeezed quadratures noise.

The modifications of the quantum noise by different types of masks are presented in Fig. 2. Based on the single-mode description of the optical field, we expected the changes in the detected quantum noise in all cases to depend only on the total optical transmission T , and to be accurately described by the beam-splitter expression:

$$SqV_{\text{out}} = 10 \cdot \log_{10}[T \cdot 10^{SqV_{\text{in}}/10} + (1 - T)], \quad (1)$$

where $SqV_{\text{in,out}}$ are the quadrature noise measured in dB before and after the mask. Clearly, the experimentally measured noise values deviated significantly from these expected dependencies; shown in Fig. 2 as dashed and dotted lines, indicating non-trivial spatial correlations [21, 22]. For example, even small losses of about 10% (for the iris mask) and 30% (for the disk mask) brought the squeezed quadrature noise significantly above shot noise. Moreover, for the disk mask even at small transmission ($T < 5\%$), the quantum noise in both quadratures was more than 5 dB above shot noise, see

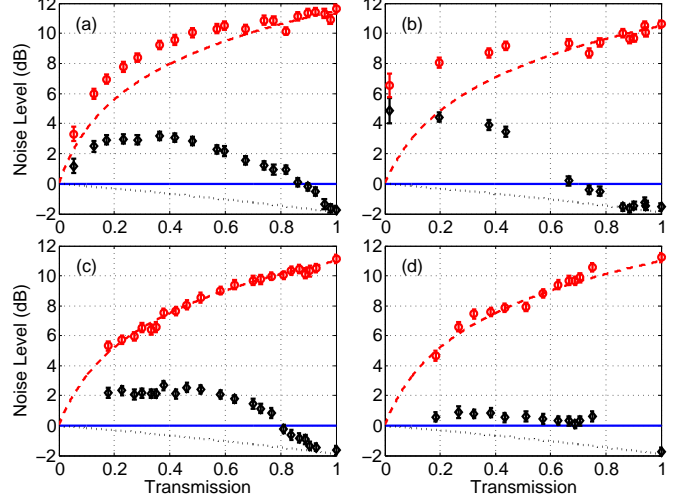


FIG. 2. (Color online) Measured minimum (diamonds) and maximum (circles) quadrature noise when the laser beam is partially blocked by (a) iris mask, (b) disk mask, (c,d) the combined masks, formed by both iris and the disk. For all measurements the horizontal axis indicates the fraction of LO intensity, transmitted through the mask. In (c) the central disk alone blocked 8% of the LO power and in (d) the power loss was 25%. Dashed and dotted lines indicate the prediction of the single-mode model, described by Eq. (1). The zero of the vertical axis corresponds to the shot-noise noise level .

Fig. 2(b). In contrast, Eq. (1) predicts that in all cases we should expect to approach the SQL monotonically from below, and to never see antisqueezing.

To gain additional insight to the spatial distribution of the squeezed vacuum field we looked at the noise of a ring-like slice of the laser beam, using the mask consisting from a fixed size opaque disk and a variable size iris. Fig. 2(c,d) represents modifications of transmitted quantum noise by such masks for the fixed disk sizes that blocked 8% and 25% of the LO power, correspondingly. Again, we were not able to improve the measured noise suppression below that of the unobstructed beam, even though the anti-squeezing noise dependence on transmission followed the uniform loss model much better. Perhaps, the ring mask was able to block especially noisy spatial modes.

The above observations suggested that generated squeezed field may consist of several spatial modes, some of which are “noisier” than others. These modes are expected to be radially symmetric due to cylindrical symmetry of our setup. The higher-order Laguerre-Gaussian (LG) modes [23] are thus natural candidates to use for the decomposition of the LO and the squeezed beam:

$$u_{l,p}(\vec{r}) = \frac{C_{l,p}}{w(z)} e^{-\frac{r^2}{w(z)^2}} e^{-\frac{ikr^2 z}{2(z^2 + z_R^2)}} \left(\frac{\sqrt{2}r}{w(z)}\right)^{|l|} \times L_p^{|l|} \left(\frac{2r^2}{w(z)^2}\right) e^{-il\phi} e^{-(2p+|l|+1)\arctan(z/z_R)} \quad (2)$$

where l is the azimuthal index and p is the radial index for each mode, $C_{l,p} = \sqrt{2p!/\pi(|l|+p)!}$ is a normalization constant, w_0 is the beam waist, $w(z) = w_0\sqrt{1+(z/z_R)^2}$ is the width of the optical field, $L_p^{|l|}$ are the generalized Laguerre polynomials, z_R is the Rayleigh range, and $k = 2\pi/\lambda$ is the wave number. Because of the conservation of the optical angular momentum, we expect that only the modes with $l = 0$ can be generated via the PSR process.

Since previous theory [12, 18] was performed in the plane-wave approximation, we have modified the PSR description to account for the possibility of the higher-order spatial modes. Following Ref. [12], we use a semi-classical theory to investigate the structure of the output beam. Treating the light classically, we start with the inhomogeneous wave equation

$$\nabla^2 \mathbf{E} - \frac{1}{c^2} \frac{\partial^2 \mathbf{E}}{\partial t^2} = \frac{1}{\epsilon_0 c^2} \frac{\partial^2 \mathbf{P}}{\partial t^2} \quad (3)$$

where $\mathbf{P} = \frac{N}{V} \langle \hat{\mathbf{d}} \rangle$ is the polarization induced in the medium and $\langle \hat{\mathbf{d}} \rangle = \langle m | \hat{\mathbf{d}} | n \rangle = \sum_{m,n} \mu_{m,n} \rho_{m,n}$ is the expectation value of the dipole operator in terms of the density matrix ρ and dipole moment μ . We use the density matrix expression for the polarization, along with the slowly varying envelope and paraxial wave approximations, to transform Eq. (3) into a propagation equation in terms of the envelope functions \tilde{E} and $\tilde{\rho}$:

$$\left(\frac{\partial}{\partial z} - \frac{i}{2k} \nabla_{\perp}^2 \right) \tilde{E} = \frac{ik}{2\epsilon_0 V} \sum_{m,n} \mu_{m,n} \tilde{\rho}_{m,n}. \quad (4)$$

Next we apply a simple model in which we treat the D1 line of ^{87}Rb as a double- Λ scheme. We treat the input field as a superposition of two circularly polarized fields characterized by Rabi frequencies Ω_+ and Ω_- , corresponding to right- and left-circular polarizations. We solve for the density matrix elements, and since our pump field is in fact linearly polarized, we convert to the linear polarization basis and distinguish the propagation equations for the two envelope functions in terms of the Rabi frequencies:

$$\hat{L} \Omega_{x,y} = -2\kappa \Omega_{x,y} \frac{|\Omega_{x,y}|^2}{|\Omega|^4} (\gamma_0 + 2i \frac{|\Omega_{x,y}|^2}{\Delta}) \quad (5)$$

where $\hat{L} \equiv \left(\frac{\partial}{\partial z} - \frac{i}{2k} \nabla_{\perp}^2 \right)$, k is the wave number, κ is the coupling constant, γ_0 is the decay rate, and Δ is the detuning. We further note that Ω_y is the Rabi frequency of the y -polarized pump field and Ω_x is the Rabi frequency of the x -polarized vacuum field. The homogeneous equation solved in cylindrical coordinates yields the LG family of solutions $u_{l,p}(\vec{r})$, given by Eq. (2). We obtain the mode structure of the output beam by avoiding a numerical calculation and proceeding with a weak scattering approximation in the following way. We assume $\Omega_{x,y}$ on the right-hand side (r.h.s.) of Eq. (5) take the

form of the input modes, i.e., $\Omega_{x,y} \rightarrow \epsilon_{x,y}^0 u_{0,0}(\vec{r})$ and use the fact that $\epsilon_x^0 \ll \epsilon_y^0$ to simplify Eq. (5):

$$\begin{aligned} \hat{L} \Omega_{x,y} = -u_{0,0}(\vec{r}) & \left[\kappa \gamma_0 \frac{\epsilon_{x,y}^0}{|\epsilon_y^0|^2} u_{0,0}(\vec{r})^* u_{0,0}(\vec{r}) \right. \\ & \left. + i \frac{\kappa}{\Delta} \epsilon_{x,y}^0 (u_{0,0}(\vec{r})^* u_{0,0}(\vec{r}))^2 \right]. \end{aligned} \quad (6)$$

In this approximation we can regard the r.h.s. of Eq. (6) as the source of the Rabi frequency on the left-hand side (l.h.s.) of Eq. (6), and with this observation we define the appropriate sources ρ_x and ρ_y to simplify the notation, i.e., we transform Eq. (5) into $\hat{L} \Omega_{x,y} = \rho_{x,y}(\vec{r})$. We can now use a Green function method [24] to write an integral expression for $\Omega_{x,y}$:

$$\begin{aligned} \Omega_{x,y} = & \int r' dr' d\phi' K(\vec{r}|\vec{r}') \Omega_{x,y}^{\text{homo}}(\vec{r}') \\ & + \int dz' \int r' dr' d\phi' G(\vec{r}|\vec{r}') \rho_{x,y}(\vec{r}') \end{aligned} \quad (7)$$

where $\Omega_{x,y}^{\text{homo}}(\vec{r}') = \epsilon_{x,y}^{\text{homo}} u_{0,0}(\vec{r})$ represents the portion of the beam passing through the cell unaltered, $K(\vec{r}|\vec{r}')$ is the propagator, and $G(\vec{r}|\vec{r}')$ is the Green function for Eq. (6). An adjustable parameter, related to the absorption and properties of the cell, characterizes the relative strength of $\rho_{x,y}$ to $\Omega_{x,y}^{\text{homo}}$. Thus, once $K(\vec{r}|\vec{r}')$ and $G(\vec{r}|\vec{r}')$ are known the problem is solved. The most effective way to write the propagator (and consequently the Green function) is in terms of the LG modes. We define the propagator and Green function accordingly:

$$\begin{aligned} K(\vec{r}|\vec{r}') \equiv & \sum_l \sum_p u_{l,p}^*(\vec{r}') u_{l,p}(\vec{r}), \\ G(\vec{r}|\vec{r}') \equiv & \Theta(z - z') K(\vec{r}|\vec{r}'). \end{aligned} \quad (8)$$

We further utilize the LG modes with an expansion of the sources $\rho_{x,y}$:

$$\begin{aligned} \rho_{x,y}(\vec{r}) = & \sum_l \sum_p c_{l,p} u_{l,p}(\vec{r}), \\ c_{l,p}(z) = & \int r dr d\phi u_{l,p}^*(\vec{r}) \rho_{x,y}(\vec{r}). \end{aligned} \quad (9)$$

We pause to point out that, since the propagation equation inherits no ϕ dependence from either the atoms or the input fields, the beam solutions will be limited to $l = 0$ modes. This is clearly seen through the integral for the $c_{l,p}$ coefficients by noting $\rho_{x,y} = \rho_{x,y}(r, z)$ and separating the ϕ phase from the LG mode:

$$c_{l,p}(z) = \int r dr \rho_{x,y}(r, z) u_{l,p}^*(r, z) \int_0^{2\pi} d\phi e^{il\phi}. \quad (10)$$

As one can see, the ϕ integral vanishes for $l \neq 0$. Using (8–10) in (7) we arrive at the final solutions for the Rabi frequencies in the weak scattering limit:

$$\Omega_{x,y} = \Omega_{x,y}^{\text{homo}}(\vec{r}) + \sum_p u_{0,p}(\vec{r}) \int_{\text{cell}} dz' c_{0,p}(z'). \quad (11)$$

By performing numerical evaluations we can verify that we explicitly retain the mode structure of the output beam and calculations show that the summation converges for $p \leq 6$.

Each of the six modes in our field has a Gouy phase. Since the Gouy phase changes most rapidly around a Gaussian beam focal point, we built a one-to-one telescope to create such a focal point, then we moved beam centered iris masks along the beam optical axis to see if the different modes have different Gouy phases as well. The modified setup is depicted in Fig. 1(b).

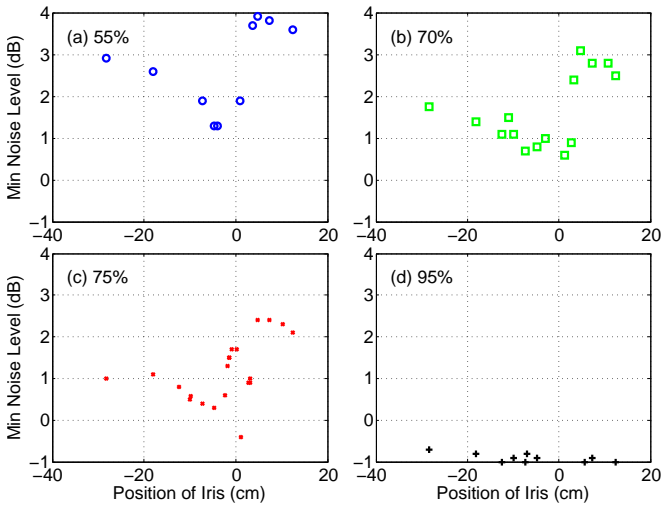


FIG. 3. (Color online) Minimum quadrature noise vs. a variable iris position. The iris size was adjusted to maintain constant transmission of the LO beam for each trace as depicted in the legend: 55% (a, circles), 70% (b, squares), 75% (c, crosses), and 95% (d, plus signs).

As we moved the iris along the beam, we change its size to maintain the same transmission of the LO beam. This allowed us to isolate our data from the beam-blocking component, since Gaussian beam cross-sections scale around the focal point similarly. So our data is mostly effected by the differential Gouy phase change in different spatial modes. We tracked the quantum noise in the maximally squeezed quadrature versus position of the iris. As one can see in Fig. 3, the quantum noise changes very drastically right around the focal point. When the iris size was large enough to allow high transmission, the noise level does not change much as the iris moved along the beam (see Fig. 3(d)). But as transmission of the mask decreased, the noise in the squeezed quadrature went above shot noise, though it noticeably decreased right around the focal point location (see Fig. 3(a, b, and c)). Perhaps the most surprising is the noise dependence for the 75% transmissive mask (see Fig. 3(c)), where one can see a very sharp drop of the noise into the global minimum around 1 cm, where it is squeezed below the shot-noise level. Similar but less pronounced behavior can be observed for the 70% transmissive mask

(see Fig. 3(b)).

In the same setup (see Fig. 1(b)), we mapped the transmission and minimum noise curve vs. the position of the fixed size iris, as shown in Fig 4. The transmission of LO exhibits some degree of asymmetry. The position of the maximum transmission shifted as we varied the iris size (see Fig. 4(a)). For the irises with 93% and 86% peak transmission, there are more than one local minima. We use Eq. (11) to predict the transmission level of the two LO field (see Fig. 4(b)), it is in a qualitatively good agreement with our experimental data (see Fig. 4(a)). The asymmetry about the focus is a result of the complex Guoy's phase structure of the solution given by Eq. (11). It is the interplay of the these phase shifts in the mode superposition that create this strange structure about the focus.

Based on the beam splitter model (Eq. (1)), we calculated the expected minimum noise as in Fig. 4(d). In the theoretical plot, the noise is always lower than shot noise since the model has no excess noise term. But, we can still compare it with Fig. 4(c) and found the overall behaviour is quite similar. In both plots, the minimum in the noise power traces shift to the right, i.e., farther from the cell as the iris size shrinks.

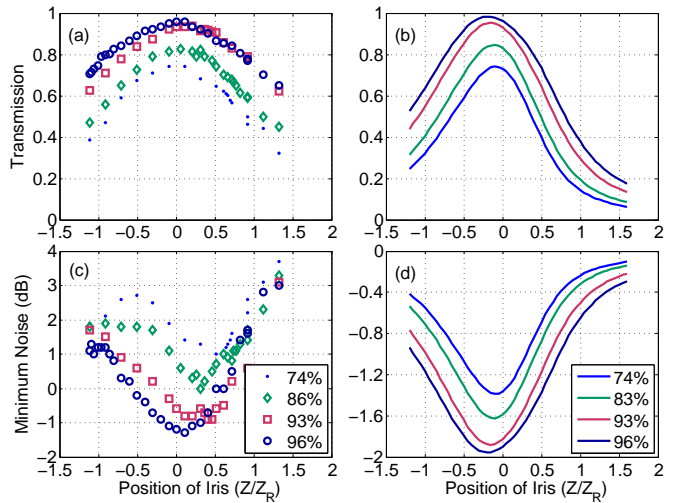


FIG. 4. (Color online) Comparison of the experimental (left column) and theoretical (right column) dependences of the LO beam transmission (top row) and the squeezed field minimal noise power (bottom row) on the iris position for several fixed iris sizes. The legend denotes the peak transmission for each iris. Note that the Rayleigh range $Z_R = 2.5$ cm. To calculate transmission and noise power, we used Eq. (11) and Eq. (1).

In conclusion, we demonstrated that the PSR squeezer generates a multi-spatial-mode squeezed field. We developed its semi-classical model, which qualitatively describes our experimental observation. Our results have application to improved single-mode squeezing and the production of squeezed light in higher-order modes upon

demand.

The authors thank G. Romanov, O. Wolfe, and T. Horrom for the assistance with the experiment. This research was supported by AFOSR grant FA9550-13-1-0098. In addition, R. N. L., Z. X. and J. P. D. acknowledge additional support from the ARO and the NSF.

* eemikh@wm.edu

- [1] N. J. Cerf, G. Leuchs, and E. S. Polzik, *Quantum Information with Continuous Variables of Atoms and Light* (Imperial College Press, London, 2007).
- [2] V. Boyer, A. M. Marino, R. C. Pooser, and P. D. Lett, *Science* **321**, 544 (2008).
- [3] J. P. Dowling, *Contemp. Phys.* **49**, 125 (2008).
- [4] M. Lassen, V. Delaubert, J. Janousek, K. Wagner, H.-A. Bachor, P. K. Lam, N. Treps, P. Buchhave, C. Fabre, and C. C. Harb, *Phys. Rev. Lett.* **98**, 083602 (2007).
- [5] G. Molina-Terriza, J. P. Torres, and L. Torner, *Nature Physics* **3**, 305 (2007).
- [6] C. Fabre, “Quantum Optics, from one mode to many modes,” (2008).
- [7] G. C. G. Berkhout, M. P. J. Lavery, J. Courtial, M. W. Beijersbergen, and M. J. Padgett, *Phys. Rev. Lett.* **105**, 153601 (2010).
- [8] O. Pinel, J. Fade, D. Braun, P. Jian, N. Treps, and C. Fabre, *Phys. Rev. A* **85**, 010101 (2012).
- [9] W. V. Davis, A. L. Gaeta, and R. W. Boyd, *Opt. Lett.* **17**, 1304 (1992).
- [10] S. M. Rochester, D. S. Hsiung, D. Budker, R. Y. Chiao, D. F. Kimball, and V. V. Yashchuk, *Phys. Rev. A* **63**, 043814 (2001).
- [11] I. Novikova, A. B. Matsko, and G. R. Welch, *Journal of Modern Optics* **49**, 2565 (2002).
- [12] A. B. Matsko, I. Novikova, G. R. Welch, D. Budker, D. F. Kimball, and S. M. Rochester, *Phys. Rev. A* **66**, 043815 (2002).
- [13] J. Ries, B. Brezger, and A. I. Lvovsky, *Phys. Rev. A* **68**, 025801 (2003).
- [14] E. E. Mikhailov and I. Novikova, *Opt. Lett.* **33**, 1213 (2008), arXiv:0802.1558.
- [15] S. Barreiro, P. Valente, H. Failache, and A. Lezama, *Phys. Rev. A* **84**, 033851 (2011).
- [16] I. H. Agha, G. Messin, and P. Grangier, *Opt. Express* **18**, 4198 (2010).
- [17] T. Horrom, R. Singh, J. P. Dowling, and E. E. Mikhailov, *Phys. Rev. A* **86**, 023803 (2012), arXiv:1202.3831.
- [18] A. Lezama, P. Valente, H. Failache, M. Martinelli, and P. Nussenzveig, *Phys. Rev. A* **77**, 013806 (2008).
- [19] T. Horrom, A. Lezama, S. Balik, M. D. Havey, and E. E. Mikhailov, *Journal of Modern Optics* **58**, 1936 (2011), arXiv:1103.1546.
- [20] M. Zhang, J. Soultanis, I. Novikova, and E. E. Mikhailov, *Opt. Lett.* **38**, 4833 (2013).
- [21] A. M. Marino, V. Boyer, R. C. Pooser, P. D. Lett, K. Lemons, and K. M. Jones, *Phys. Rev. Lett.* **101**, 093602 (2008).
- [22] A. Marino, J. Clark, Q. Glorieux, and P. Lett, *The European Physical Journal D* **66**, 288 (2012), 10.1140/epjd/e2012-30037-1.
- [23] A. Siegman, *Lasers* (University Science Books, Sausalito CA, 1986).
- [24] G. Barton, *Elements of Green's Functions and Propagation* (Oxford University Press, New York NY, 1989).